New Journal of Physics
The open-access journal for physics

Magnetic Kronig–Penney model for Dirac electrons in single-layer graphene

M Ramezani Masir[1], **P Vasilopoulos**[2] **and F M Peeters**[1,3,4]

[1] Departement Fysica, Universiteit Antwerpen, Groenenborgerlaan 171, B-2020 Antwerpen, Belgium
[2] Department of Physics, Concordia University, 7141 Sherbrooke Street West Montreal, Quebec, H4B 1R6, Canada
[3] Departamento de Física, Universidade Federal do Ceará, Caixa Postal 6030, Campus do Pici, 60455-760 Fortaleza, Ceará, Brazil
E-mail: mrmphys@gmail.com, takis@alcor.concordia.ca and francois.peeters@ua.ac.be

New Journal of Physics **11** (2009) 095009 (21pp)
Received 7 May 2009
Published 30 September 2009
Online at http://www.njp.org/
doi:10.1088/1367-2630/11/9/095009

Abstract. The properties of Dirac electrons in a magnetic superlattice (SL) on graphene consisting of very high and thin (δ-function) barriers are investigated. We obtain the energy spectrum analytically and study the transmission through a finite number of barriers. The results are contrasted with those for electrons described by the Schrödinger equation. In addition, a collimation of an incident beam of electrons is obtained along the direction perpendicular to that of the SL. We also highlight an analogy with optical media in which the refractive index varies in space.

[4] Author to whom any correspondence should be addressed.

Contents

1. Introduction

During the last five years single-layer graphene (a monolayer of carbon atoms) has become a very active field of research in nanophysics [1, 2]. It is expected that this material will serve as a base for new electronic and opto-electric devices. The reason is that graphene's electronic properties are drastically different from those, say, of conventional semiconductors. Charge carriers in a wide single-layer graphene behave like 'relativistic', chiral and massless particles with a 'light speed' equal to the Fermi velocity and possess a *gapless, linear* spectrum close to the K and K' points. One major consequence is the perfect transmission through arbitrarily high and wide barriers, referred to as Klein tunneling.

One of the most challenging tasks is to learn how to control the electron behavior using electric fields in graphene. This task is made complicated precisely by the Klein tunneling according to which Dirac electrons in graphene can tunnel through arbitrarily wide and high electric barriers [3].

Alternatively, one can apply a magnetic field to control the electron motion. It has been shown in numerous papers that an inhomogeneous magnetic field can confine standard electrons described by the Schrödinger equation [4]–[6]. The question then arises whether it can confine Dirac electrons in graphene. Up to now semi-infinite magnetic structures, that are homogeneous in one direction, have been considered, making the task simpler by converting the problem into a one-dimensional (1D) one [7]–[15]. In particular, magnetic confinement of Dirac electrons in graphene has been reported in structures involving one [7] or several magnetic barriers [8, 9] as well as in superlattices (SLs), without magnetic field for some very special values of the parameters involved [16]. In such structures standard electrons can remain close to the interface and move along so-called snake orbits [5] or in pure quantum mechanical unidirectional states [4].

Given the importance of graphene, it would be appropriate to study this magnetic confinement more systematically. We make such a study here by considering a *magnetic* Kronig–Penney (KP) model in graphene, i.e. a series of magnetic δ-function barriers that

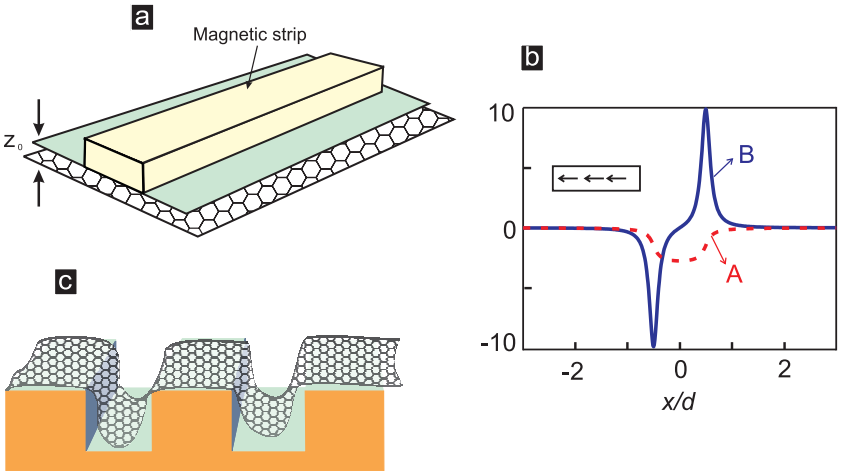

Figure 1. (a) Layout of the system: a ferromagnetic strip on the top of a bilayer graphene sheet separated by a thin oxide layer. (b) Magnetic field and corresponding vector potential at a distance $z_0 = 0.1$ under the strip parallel to it. (c) A graphene layer on the top of a periodic structured surface.

alternate in sign. This model can be realized experimentally in two different ways:

1. One can deposit ferromagnetic strips on the top of a graphene layer but in a way that there is no electrical contact between graphene and these strips. When one magnetizes the strips along the x direction, cf figure 1(a), by e.g. applying an in-plane magnetic field, the charge carriers in the graphene layer feel an inhomogeneous magnetic field profile. This profile can be well approximated [22] by $2B_0 z_0 h/d(x^2 + z_0^2)$ on one edge of the strip and by $-2B_0 z_0 h/(x^2 + z_0^2)$ on the other, where z_0 is the distance between the two-dimensional electron gas (2DEG) and the strip, and d and h the width and height of the strip (see figure 1(b)). The resulting magnetic field profile will be modeled by two magnetic δ-functions of height $2\pi B_0 h$. Such ferromagnetic strips were deposited on the top of a 2DEG in a semiconductor heterostructure in [23].
2. It was recently shown that local strain in graphene induces an effective inhomogeneous magnetic field [24] (figure 1(c)). When one puts the graphene layer on a periodically structured substrate the graphene at the edges of the substrate becomes strained and the situation can be described by a magnetic δ-function profile such as that shown in figure 2.

In a quantum mechanical treatment of the above two systems, the vector potential $\mathbf{A}(x)$ is the essential quantity and, within the Landau gauge, $\mathbf{A}(x)$ is nothing else than a periodic array of step functions. The Hamiltonian describing this system is periodic and consequently we expect the energy spectrum of the charge carriers in graphene to exhibit a band structure. The advantage of this *magnetic* KP model is mainly its analytical simplicity that provides some insight and allows a contrast with the same model for standard electrons [27]. To do that we adapt a method developed in optics, for a medium with a periodic-in-space refractive index. This optical method is clear and very well suited to the problem. Incidentally, there are many analogues of optical behavior in electronics, such as focusing [17]–[19], [30], [31], collimation or quasi-1D motion of electrons and photons [4, 8, 16, 20], and interference [21] in a 2DEG.

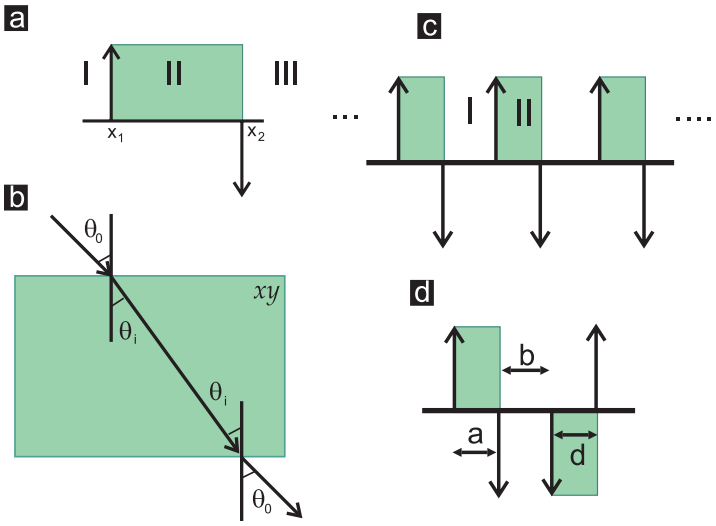

Figure 2. (a) Two opposite magnetic δ-function barriers, indicated by arrows; the vector potential is shown by the shaded (green) area. (b) Angles related to the propagation of an electron through this system. (c) Schematics of a periodic vector potential (shaded areas) and corresponding magnetic field indicated by the black arrows. (d) Arrangement of magnetic δ-functions that leads to a periodic and alternating in sign vector potential.

The paper is organized as follows. In section 2, we present the method and evaluate the spectrum and electron transmission through two antiparallel, δ-function magnetic barriers. In section 3, we consider SLs of such barriers and present numerical results for the energy spectrum. In section 4, we consider a series of δ-function vector potentials and our concluding remarks are given in section 5.

2. Characteristic matrix for Dirac electrons

An electron in a single-layer graphene, in the presence of a perpendicular magnetic field $B(x)$, which depends on x, is adequately described by the Hamiltonian

$$H_0 = v_F \sigma \cdot (\mathbf{p} + e\mathbf{A}(x)), \tag{1}$$

where $\mathbf{p}$ is the momentum operator, v_F the Fermi velocity, and $\mathbf{A}(x)$ the vector potential. To simplify the notation, we introduce the dimensionless units: $\ell_B = [\hbar/eB_0]^{1/2}$, $B(x) \to B_0 B(x)$, $\mathbf{A}(x) \to B_0 \ell_B \mathbf{A}(x)$, $t \to t\ell_B/v_F$, $\vec{r} \to \ell_B \vec{r}$, $\vec{v} \to v_F \vec{v}$, $E \to E_0 E$, $u(x) \to E_0 u(x)$, and $E_0 = \hbar v_F/\ell_B$. Here ℓ_B is the magnetic length and t the tunneling strength. In these units equation (1) takes the form

$$H = \begin{pmatrix} 0 & \partial_x - \mathrm{i}\partial_y + A(x) \\ \partial_x + \mathrm{i}\partial_y - A(x) & 0 \end{pmatrix}. \tag{2}$$

Then the equation $H\Psi(x, y) = E\Psi(x, y)$ admits solutions of the form

$$\Psi(x, y) = \begin{pmatrix} \psi_I(x, y) \\ \psi_{II}(x, y) \end{pmatrix}, \tag{3}$$

with $\psi_{\rm I}(x, y)$, $\psi_{\rm II}(x, y)$ obeying the coupled equations

$$\mathrm{i}\left[\frac{\partial}{\partial x} - \mathrm{i}\frac{\partial}{\partial y} + A(x)\right]\psi_{\rm II} + E\psi_{\rm I} = 0, \tag{4}$$

$$\mathrm{i}\left[\frac{\partial}{\partial x} + \mathrm{i}\frac{\partial}{\partial y} - A(x)\right]\psi_{\rm I} + E\psi_{\rm II} = 0. \tag{5}$$

Due to the translational invariance along the y direction, we assume solutions of the form $\Psi(x, y) = \exp \mathrm{i}k_y y(U(x), V(x))^{\rm T}$, with the superscript 'T' denoting the transpose of the row vector. For $B(x) \sim \delta(x)$, the corresponding vector potential is a step function $A(x) \sim \Theta(x)$. For $A(x) = P$ constant, equations (4) and (5) take the form

$$\left[\frac{\mathrm{d}}{\mathrm{d}x} + (k_y + P)\right]V = \mathrm{i}EU, \tag{6}$$

$$\left[\frac{\mathrm{d}}{\mathrm{d}x} - (k_y + P)\right]U = \mathrm{i}EV, \tag{7}$$

Equations (3)–(7) correspond to those for an electromagnetic wave propagating through a medium in which the refractive index varies periodically. The two components of $\Psi(x, y)$ correspond to those of the electric (or magnetic) field of the wave [28, 29].

Equations (6) and (7) can be readily decoupled by substitution. The result is

$$\frac{\mathrm{d}^2 Z}{\mathrm{d}x^2} + \left[E^2 - (k_y + P)^2\right]Z = 0, \tag{8}$$

where $Z = U, V$. If $E^2 \to E'$ and $(k_y + P)^2 \to V_{\rm eff}$, equation (8) reduces to a Schrödinger equation for a standard electron where $V_{\rm eff}(k_y, x) = (k_y + P)^2$ can be considered as an effective potential. Taking θ_0 as the angle of incidence, we have $k_x = E\cos\theta_0 = [E^2 - k_y^2]^{1/2}$ and $k_y = E\sin\theta_0$ as the wave vector components outside the medium and $k'_x = E\cos\theta = [E^2 - (k_y + P)^2]^{1/2}$ as the electron wave vector inside the medium; $\theta = \tan^{-1}(k_y/k'_x)$ is the refraction angle. This renders equation (8) simpler with acceptable solutions for U and V

$$U(x) = A\cos(Ex\cos\theta) + B\sin(Ex\cos\theta), \tag{9}$$

$$V(x) = -\mathrm{i}\{B\cos(\theta + Ex\cos\theta) - A\sin(\theta + Ex\cos\theta)\}. \tag{10}$$

For future purposes, we write U and V as a linear combination of U_1, U_2 and V_1, V_2:

$$\begin{aligned} &\frac{\mathrm{d}V_1}{\mathrm{d}x} + (k_y + P)V_1 = \mathrm{i}EU_1, \qquad \frac{\mathrm{d}V_2}{\mathrm{d}x} + (k_y + P)V_2 = \mathrm{i}EU_2. \\ &\frac{\mathrm{d}U_1}{\mathrm{d}x} - (k_y + P)U_1 = \mathrm{i}EV_1, \qquad \frac{\mathrm{d}U_2}{\mathrm{d}x} - (k_y + P)U_2 = \mathrm{i}EV_2. \end{aligned} \tag{11}$$

We now multiply the equations of the first row by U_2 and U_1, respectively, and those of the second by V_2 and V_1. The resulting equations lead to

$$\frac{\mathrm{d}\mathbf{D}}{\mathrm{d}x} = U'_1V_2 + U_1V'_2 - V'_1U_2 - V_1U'_2 = 0, \tag{12}$$

where $\mathbf{D} = \det D$ and

$$D = \begin{pmatrix} U_1 & V_1 \\ U_2 & V_2 \end{pmatrix}. \tag{13}$$

Equation (12) shows that the determinant of the matrix (13) associated with any two arbitrary solutions of equation (8) is a constant, i.e. D is an invariant of the system of equations (11). This also follows from the well-known property of the Wronskian of second-order differential equations. For our purposes a convenient choice of particular solutions is

$$\begin{aligned} U_1 &= f(x), \qquad U_2 = F(x), \\ V_1 &= g(x), \qquad V_2 = G(x), \end{aligned} \tag{14}$$

such that

$$f(0) = g(0) = 0, \quad F(0) = G(0) = 1. \tag{15}$$

Then the solution, with $U(0) = U_0$ and $V(0) = V_0$, can be expressed as

$$U = FU_0 + fV_0, \quad V = GU_0 + gV_0 \tag{16}$$

or, in matrix notation, as

$$\mathbf{Q} = \begin{bmatrix} U(x) \\ V(x) \end{bmatrix}, \qquad \mathbf{Q}_0 = \begin{bmatrix} U_0 \\ V_0 \end{bmatrix}, \qquad \mathbf{N} = \begin{bmatrix} F(x) & f(x) \\ G(x) & g(x) \end{bmatrix}. \tag{17}$$

Since D is constant, the determinant of the square matrix N is a constant; its value, found by setting $x = 0$, is $\det N = Fg - fG = 1$. It is usually more convenient to express U_0 and V_0 as a function of $U(x)$ and $V(x)$. Solving for U_0 and V_0, we obtain $\mathbf{Q}_0 = \mathbf{MQ}$, where

$$\mathbf{M}(x) = \begin{bmatrix} g(x) & -f(x) \\ -G(x) & F(x) \end{bmatrix}. \tag{18}$$

This matrix $\mathbf{M}$ is unimodular, $|\mathbf{M}| = 1$. Now we can find the characteristic matrix from equations (9) and (10) as

$$\mathbf{M}(x) = \frac{1}{\cos\theta} \begin{bmatrix} \cos(\theta + Ex\cos\theta) & -\mathrm{i}\sin(Ex\cos\theta) \\ -\mathrm{i}\sin(Ex\cos\theta) & \cos(\theta - Ex\cos\theta) \end{bmatrix}. \tag{19}$$

2.1. Bound states

With regard to the average of vector potential we shall consider two different systems: one with zero average and the other with nonzero average along the x direction. First let us consider the magnetic field profile as shown in figure 2(a) for which the corresponding vector potential is

$$A(x) = P\Theta(x)\Theta(L - x), \tag{20}$$

where $\Theta(x) = 0(x < 0),\ 1(x > 0)$ is the theta function. This vector potential has a nonzero average, and the corresponding effective potential becomes (see figure 3(a)) as

$$V_{\mathrm{eff}}(k_y, x) \sim \begin{cases} k_y^2, & -x < 0, \\ (k_y + P)^2, & 0 < x < L, \\ k_y^2, & x > L. \end{cases} \tag{21}$$

Here L is measured in units of the magnetic length l_{B}. There are two different cases that we have to consider.

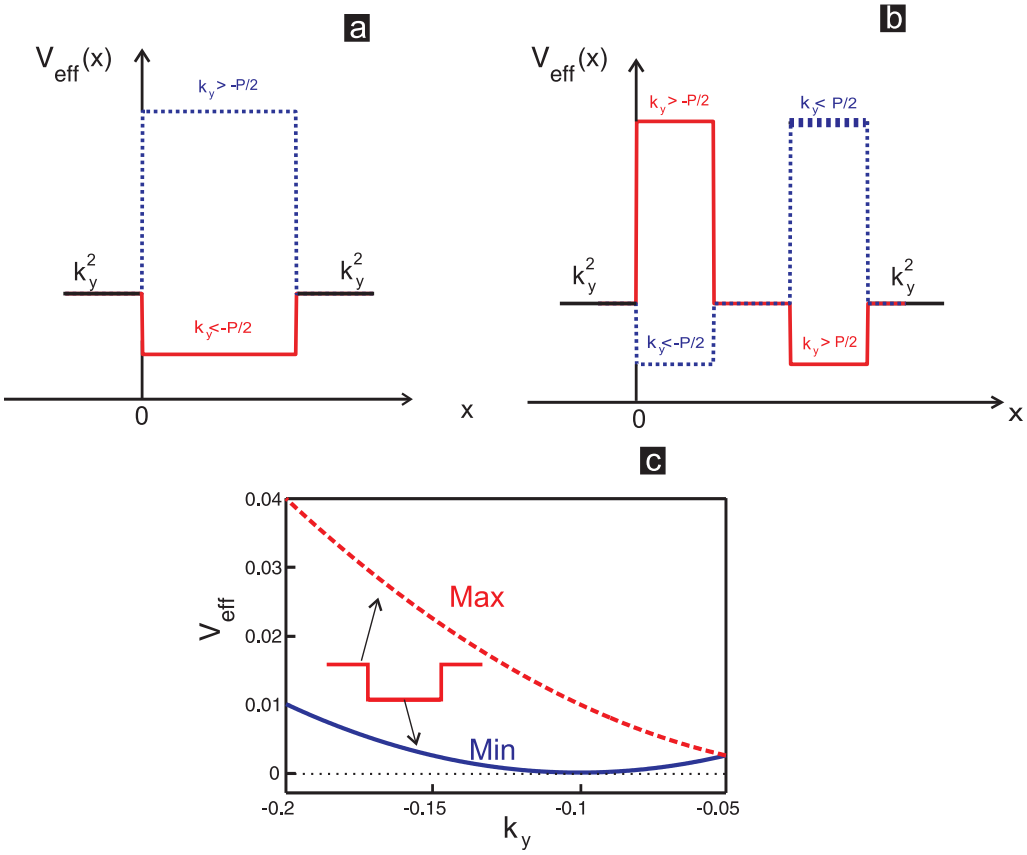

Figure 3. The effective potential for $k_y < -P/2$ and $k_y > P/2$ for two different cases, (a) vector potential with nonzero average corresponding to figure 2(a), and (b) vector potential with zero average corresponding to figure 2(c). (c) Minimum (blue full curve) and maximum (red dashed curve) of the effective potential versus k_y corresponding to the situation depicted in (a) for $P = 0.1$.

Case 1 for $k_y < -P/2$: as shown in figure 3(a) by the full red curve, we have a 1D symmetric quantum well that, as is well-known, has at least one bound state (see also figure 3(c)). For $E^2 < k_y^2$, the particle will be bound, while for $E^2 > k_y^2$, we have scattered states, or equivalently the electron tunnels through the magnetic barriers.

Case 2 for $k_y > -P/2$: as shown in figure 3(a) by the dotted blue curve, the effective potential is similar to that of a barrier. We have a pure tunneling problem. With reference to figure 2, $x_1 = 0$ and $x_2 = L$, the solutions are as follows. For $x < 0$, the wave function is

$$\psi(x) = C\mathrm{e}^{\kappa x}\begin{pmatrix} 1 \\ -\mathrm{i}\mathrm{e}^{-\xi} \end{pmatrix}, \tag{22}$$

where $\kappa = E\cosh\xi$ and $k_y = E\sinh\xi$, while for $x > L$ it is

$$\psi(x) = D\mathrm{e}^{-\kappa x}\begin{pmatrix} 1 \\ \mathrm{i}\mathrm{e}^{\xi} \end{pmatrix}. \tag{23}$$

In the middle region, $0 < x < L$, the wave function is given by

$$\psi(x) = F\mathrm{e}^{\mathrm{i}k'x}\begin{pmatrix} 1 \\ \mathrm{e}^{\mathrm{i}\theta} \end{pmatrix} + Q\mathrm{e}^{-\mathrm{i}k'x}\begin{pmatrix} 1 \\ -\mathrm{e}^{-\mathrm{i}\theta} \end{pmatrix}, \tag{24}$$

with $k' = [E^2 - (k_y + P)^2]^{1/2} = E\cos\theta$. Matching the wave functions at $x = 0$ and $x = L$ leads to a system of four equations relating the coefficients C, D, F and Q. Setting the determinant of these coefficients equal to zero, we obtain a transcendental equation whose solution gives the energy spectrum

$$\cos\theta \cosh\xi \cos k'L + \sin\theta \sinh\xi \sin k'L = 0. \tag{25}$$

For the special value of $k_y = -P$, we have $\sin\theta = 0$ and can rewrite equation (25) as $\cos(EL) = 0$ or equally $E_n = (n + \frac{1}{2})\frac{\pi}{L}$. The resulting bound states, as a function of k_y, are shown by the red full curves in figure 4(a). The area of existence of bound states is delimited by the lines $E = -k_y$ and $E = -(k_y + P)$. The number of bound states increases with $|k_y|$ which is also clear from the behavior of the minimum and maximum of the effective potential (see figure 3(c)). No bound states are found for $k_y > -P/2$ as is also apparent from figure 3(c). For $k_y \to -P/2$, the potential is shallow and only one bound state exists. The average velocity $v_n(k_y)$ along the y direction is given by

$$v_n(k_y) = \partial E/\partial k_y = \int_{-\infty}^{+\infty} \mathrm{d}x\ j_y(x), \tag{26}$$

where $j_y = -\mathrm{i}(U^*V - V^*U)$. From figure 4(a) it is clear that these bound states move along the y direction, i.e. along the magnetic barriers. Their velocity $v_y > -v_\mathrm{F}$ is negative for $k_y < -P$, but as the electron is approaching $k_y \to -P$ we have $v_y \to 0$. For $k_y > -P$, the velocity $v_y > v_\mathrm{F}$ is positive. This can be understood from the maximum and minimum of the effective potential which is shown in figure 3(c). The energy bound states can only exist between these two lines. Note that the slope of min V_eff is negative for $k_y < -P$, while it turns positive for $k_y > -P$, which explains the k_y dependence of the velocity. From figure 4(a) it is clear there are two different classes of bound states. The bound state that follows very closely the $k_y = -P$ curve and extends to the region $-P < k_y < 0$ with energy close to zero has a wave function that is concentrated around the position of the two magnetic delta-functions and decays exponentially in the region $0 < x < L$. The wave functions of the other bound states are concentrated in a region between the two magnetic delta-functions (i.e. in a standing wave fashion) and decay exponentially outside this region.

Next, we consider a structure with zero-average vector potential as shown in figure 2(b), with corresponding effective potential shown in figure 3(b). The effective potential for $k_y < -P/2$ and $k_y > P/2$ consists of a potential well and a potential barrier and therefore has at least one bound state. Thus, we expect bound states for all k_y with energy between $E = -(+)(k_y + P)$ and $E = -(+)k_y$ when $k_y < -P/2$ ($k_y > P/2$). The dispersion relation for those bound states results from the solution of

$$M_{21} - M_{12} - \mathrm{i}M_{22}\mathrm{e}^{-\xi} - \mathrm{i}M_{11}\mathrm{e}^{\xi} = 0, \tag{27}$$

where $\mathbf{M}$ is the transfer matrix for the unit shown in figure 2(d). These bound states are shown by the red full curves in figure 4(b). Because of the spatial inversion symmetry of the vector potential the spectrum has the symmetry $E(-k_y) = E(k_y)$. Note that for $-P < k_y < P$ the lowest bound state has energy $E \approx 0$. For $-P/2 < k_y < P/2$, we have two potential barriers and therefore no bound states.

2.2. Reflection and transmission coefficients

Consider a plane wave incident upon a system of two δ-function magnetic barriers, identical in height but opposite in direction, placed at $x = 0$ and $x = L$, as shown schematically in

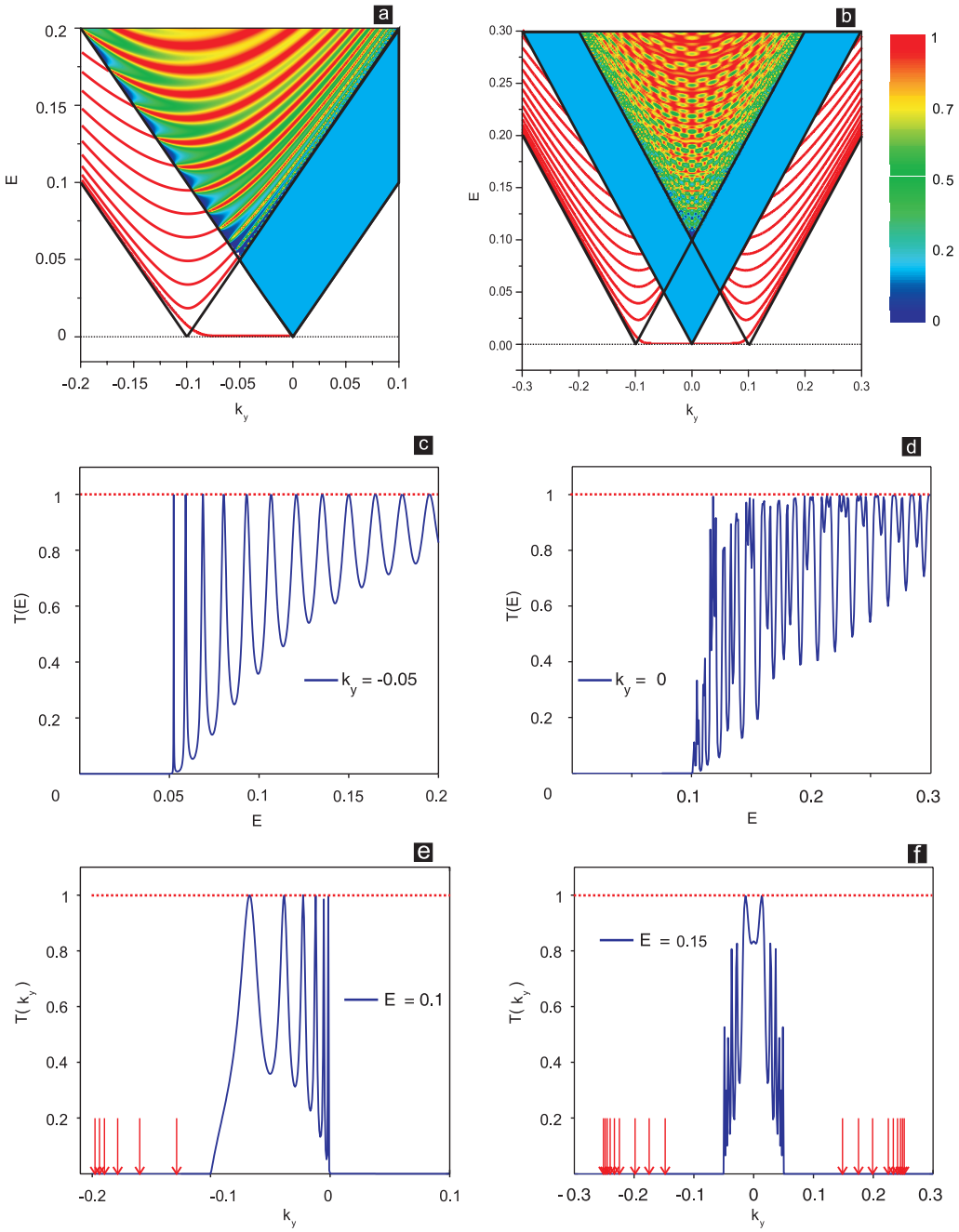

Figure 4. (a) Energy spectrum (red full curves on white background) and contour plot of the transmission (color background) through two magnetic, but opposite in direction δ-function barriers for $L = 200$ and $P = 0.1$. (b) The same as (a) but now for the configuration shown in figure 2(b) for $a = b = c = 200$ and $P = 0.1$. (c) Transmission versus energy through the magnetic δ-function barriers in (a) for $k_y = -0.05$. (d) Same as (c) but now for the configuration shown in figure 2(b) for $k_y = 0$. (e) Transmission versus k_y through the system described in (a) for fixed $E = 0.1$. The red arrow lines indicate the position of the bound states. (f) Same as (e) but now for the configuration shown in figure 2(b) for $E = 0.15$.

figure 2(a). In this case, the vector potential is constant for $0 \leqslant x \leqslant L$, zero outside this region, and homogeneous in the y direction. Below we derive expressions for the amplitudes and intensities of the reflected and transmitted waves.

Let A, R and T denote the amplitudes of the incident, reflected and transmitted waves, respectively. Further, let θ_0 be the angle of incidence and exit as shown in figure 2(b). The boundary conditions give

$$\begin{aligned} U_0 &= A + R, & U(L) &= T\mathrm{e}^{\mathrm{i}kL}, \\ V_0 &= A\mathrm{e}^{\mathrm{i}\theta_0} - R\mathrm{e}^{-\mathrm{i}\theta_0}, & V(L) &= \mathrm{e}^{\mathrm{i}\theta_0}\mathrm{e}^{\mathrm{i}kh}T. \end{aligned} \tag{28}$$

The four quantities U_0, V_0, U and V given by equations (28) are connected by the basic relation $\mathbf{Q}_0 = \mathbf{MQ}$; hence, with $J = m'_{11} + m'_{12}\mathrm{e}^{\mathrm{i}\theta_0}$ and $K = m'_{21} + m'_{22}\mathrm{e}^{\mathrm{i}\theta_0}$, we have

$$A + R = JT\mathrm{e}^{\mathrm{i}kL}, \qquad A\mathrm{e}^{\mathrm{i}\theta_0} - R\mathrm{e}^{-\mathrm{i}\theta_0} = KT\mathrm{e}^{\mathrm{i}kL}, \tag{29}$$

where m'_{ij} are the elements of the characteristic matrix of the medium, evaluated at $x = L$. From equation (29) we obtain the reflection and transmission amplitudes

$$r = \frac{R}{A} = \frac{J\mathrm{e}^{\mathrm{i}\theta_0} - K}{J\mathrm{e}^{-\mathrm{i}\theta_0} + K}, \qquad t = \frac{T}{A} = \frac{2\mathrm{e}^{-\mathrm{i}kh}\cos\theta_0}{J\mathrm{e}^{-\mathrm{i}\theta_0} + K}. \tag{30}$$

In terms of r and t, the *reflectivity* and *transmissivity* are

$$\mathcal{R} = |r|^2, \qquad \mathcal{T} = |t|^2. \tag{31}$$

The characteristic matrix for a homogeneous vector potential is given by equation (19). Labeling with subscripts 1, 2 and 3 quantities which refer to the regions, respectively, I, II and III of figure 2(a), and by $L = x_2 - x_1$ the distance between the magnetic δ-functions, we have ($\beta = EL\cos\theta_i$)

$$\begin{aligned} m'_{11} &= \cos(\theta_i + \beta)/\cos\theta_i, & m'_{22} &= \cos(\theta_i - \beta)/\cos\theta_i, \\ m'_{12} &= -\mathrm{i}\sin\beta/\cos\theta_i, & m'_{21} &= -\mathrm{i}\sin\beta/\cos\theta_i. \end{aligned} \tag{32}$$

The reflection and transmission amplitudes r and t are obtained by substituting these expressions in those for J and K that appear in equation (30). The resulting formula can be expressed in terms of the amplitudes r_{12}, t_{12} and r_{23}, t_{23} associated with the reflection at and transmission through the first and second 'interface', respectively. We have

$$r_{12} = \frac{\mathrm{e}^{\mathrm{i}\theta_0} - \mathrm{e}^{\mathrm{i}\theta_i}}{\mathrm{e}^{-\mathrm{i}\theta_0} + \mathrm{e}^{\mathrm{i}\theta_i}}, \qquad t_{12} = \frac{2\cos\theta_0}{\mathrm{e}^{-\mathrm{i}\theta_0} + \mathrm{e}^{\mathrm{i}\theta_i}} \tag{33}$$

and similar expressions for r_{23} and t_{23}. In terms of these, expressions r and t become

$$r = \frac{r_{12} + r_{23}\mathrm{e}^{2\mathrm{i}\beta}}{1 + r_{12}r_{23}\mathrm{e}^{2\mathrm{i}\beta}}, \qquad t = \frac{t_{12}t_{23}\mathrm{e}^{\mathrm{i}\beta}}{1 + r_{12}r_{23}\mathrm{e}^{2\mathrm{i}\beta}}. \tag{34}$$

The amplitude t of the transmission through the system is given by [8, 9, 12, 24, 25],

$$t = \frac{2\mathrm{e}^{-\mathrm{i}kL}\cos\theta_0\cos\theta_i}{\mathrm{e}^{-\mathrm{i}\beta}[\cos(\theta_0 + \theta_i) + 1] + \mathrm{e}^{\mathrm{i}\beta}[\cos(\theta_0 - \theta_i) - 1]}, \tag{35}$$

where $k_y = E\sin\theta_0$ and $k_y + P = E\sin\theta_i$. This equation remains invariant under the changes $E \to -E$, $\theta_0 \to -\theta_0$ and $\theta_i \to -\theta_i$. A contour plot of the transmission is shown in figure 4(a) and slices for constant k_y and E are shown, respectively, in figures 4(c) and (d). By imposing

the condition that the wave number k_x be real for incident and transmitted waves, we find that the angles θ_0 and θ_i are related by

$$\sin\theta_0 + P/E = \sin\theta_i. \tag{36}$$

Equation (36) expresses the angular confinement of the transmission elaborated in [8, 9, 12, 25, 26]. Notice its formal similarity with Snell's law. Using equation (36) we obtain the range of the angles of incidence θ_0 for which transmission through the first magnetic barrier is possible

$$-1 - P/E \leqslant \sin\theta_0 \leqslant 1 - P/E. \tag{37}$$

For the special value of the energy $E = P/2$ and θ_0 in the range $-\pi/2 \leqslant \theta_0 \leqslant \pi/2$, we have $\theta_i = \pi/2$, while for $E = -P/2$ the result is $\theta_i = -\pi/2$. Alternatively, we can put $\theta_i = \pm\pi/2$ in equation (36) and obtain, for $P > 0$, the result

$$\sin\theta_0^{\pm} = \pm 1 - P/E, \tag{38}$$

where the $+(-)$ sign corresponds to $E > 0$ ($E < 0$). A contour plot of the transmission as function of E and k_y, obtained from equation (35), is shown in figure 4(a). In figure 4(a), we distinguish three different regions. In the region between $E = -(k_y + P/2)$ and $E = -k_y$, the wavevector of the incident wave is imaginary and they are evanescent waves. In this region, k' is real and it is possible to find localized states. The k and k' for the second region between $E = k_y + P/2$ and $E = -(k_y - P/2)$ are real and the electron can tunnel through the magnetic δ-barriers. In the blue shadow region between $E = k_y + P/2$ and $E = k_y - P/2$, k is real but k' is imaginary and solutions inside the barrier are evanescent and there is very little tunneling which very quickly becomes zero. The transmission probability $|T| = t \cdot t^*$ is equal to 1 for $\cos(2\beta) = 1$. In this case, the energy becomes

$$E_n = \pm\left[n^2\pi^2/L^2 + (k_y + P)^2\right]^{1/2}, \qquad n = 1, 2, \ldots. \tag{39}$$

The condition $\cos(2\beta) = 1$, or equivalently $\beta = n\pi = Eh\cos\theta_2$ with n an integer, should be combined with that for the transmission to occur in the region delimited by the curves $E = \pm(k_y + P)$ and $E = \pm k_y$. For example, in figure 4(a) for $k_y = -0.05$ and $0 < E < 0.2$ we have 12 maxima. It is readily seen that with these parameters in equation (39) we find 12 different energies as shown in figure 4(c).

Figure 4(b) shows a contour plot of the transmission for the structure shown in figure 2(d), which is symmetric around $k_y = 0$. Note that the number of resonances has increased substantially as compared to the previous case which is due to the fact that we have twice as many magnetic barriers in our systems.

3. A series of units with magnetic δ-function barriers

3.1. N units

We consider a system of N units, such as those shown in figures 2(a) and (d) with periods $L = a + b$ and $L = a + b + c + d$, respectively. The corresponding periodic vector potential is $\mathbf{A}(x) = \mathbf{A}(x + nL)$ and the magnetic field $\mathbf{B} = \mathbf{B}(x + nL)$, with $n = 1, 2, \ldots, N$. The characteristic matrix for one period $\mathbf{M}(L)$ is denoted by

$$\mathbf{M}(L) = \begin{bmatrix} m_{11} & m_{12} \\ m_{21} & m_{22} \end{bmatrix}. \tag{40}$$

On account of the periodicity we have

$$\mathbf{M}(NL) = \underbrace{\mathbf{M}(L)\cdot\mathbf{M}(L)\ldots\mathbf{M}(L)}_{N \text{ factors}} = (\mathbf{M}(L))^N. \tag{41}$$

To evaluate the elements of $\mathbf{M}(NL)$ we use a result from the theory of matrices, according to which the Nth power of a unimodular matrix $\mathbf{M}(L)$ is ($u_N(\chi) \equiv u_N$)

$$[\mathbf{M}(L)]^N = \begin{bmatrix} m_{11}u_{N-1} - u_{N-2} & m_{12}u_{N-1} \\ m_{21}u_{N-1} & m_{22}u_{N-1} - u_{N-2} \end{bmatrix}, \tag{42}$$

with $\chi = \frac{1}{2}\,\mathrm{Tr}\,\mathbf{M}$ and u_N the Chebyshev polynomials of the second kind:

$$u_N(\chi) = \sin[(N+1)\zeta]/\sin\zeta, \tag{43}$$

where

$$\zeta = \cos^{-1}\chi, \tag{44}$$

Here ζ is the *Bloch phase* of the periodic system [33], which is related to the eigenfunctions of $\mathbf{M}$. In the limiting case of $N \to \infty$, we have total reflection when ζ is outside the range $(-1, 1)$.

3.2. SL

Here we consider a finite number N of lattice units shown in figure 2(c). We set

$$\begin{aligned} &\beta_2 = Eb\cos\theta_2, \quad \beta_1 = Ea\cos\theta_1, \quad p_2 = 1/\cos\theta_2, \\ &p_1 = 1/\cos\theta_1, \quad h = a+b, \quad \lambda_n^{\pm} = \theta_n \pm \beta_n. \end{aligned} \tag{45}$$

The characteristic matrix $\mathbf{M}_2(L)$ for one period is readily obtained, in terms of these quantities, as in section 2, and from that the characteristic matrix $\mathbf{M}_{2N}(NL)$ of the multilayer system according to equation (41). Its elements are

$$\begin{aligned} M_{11} &= s[\cos\lambda_2^+\cos\lambda_1^+ - \sin\beta_2\sin\beta_1]u_{N-1} - u_{N-2}, \\ M_{12} &= -\mathrm{i}s[\cos\lambda_2^+\sin\beta_1 + \sin\beta_2\cos\lambda_1^-]u_{N-1}, \\ M_{21} &= -\mathrm{i}s[\cos\lambda_1^+\sin\beta_2 + \sin\beta_1\cos\lambda_2^-]u_{N-1}, \\ M_{22} &= s[\cos\lambda_2^-\cos\lambda_1^- - \sin\beta_2\sin\beta_1]u_{N-1} - u_{N-2}, \end{aligned} \tag{46}$$

where $s = p_2p_1$, $u_N \equiv u_N(\chi)$, and

$$\chi = \cos(k_1a)\cos(k_2b) - \left(\frac{k_2^2 + k_1^2 + P^2}{2k_2k_1}\right)\sin(k_1a)\sin(k_2b). \tag{47}$$

The reflection and transmission coefficients of the multi-unit system are immediately obtained by substituting these expressions into equation (30). The numerical results are shown in figures 5 and 6 for finite SL with $N = 10$ units. Two different types of structures are considered as shown in the insets to figures 6. The transmission does not have $k_y \to -k_y$ symmetry for the periodic system with magnetic delta up-down as is apparent from figure 6(a). We contrast these results with the case in which we used an arrangement of magnetic delta-function as in the previous structure plus another unit with an opposite direction of magnetic delta-function. As is clearly shown in figure 6(b), we have $k_y \to -k_y$ symmetry for the transmission probability through this structure. The transmission resonances are more pronounced, i.e. the dips become deeper, when

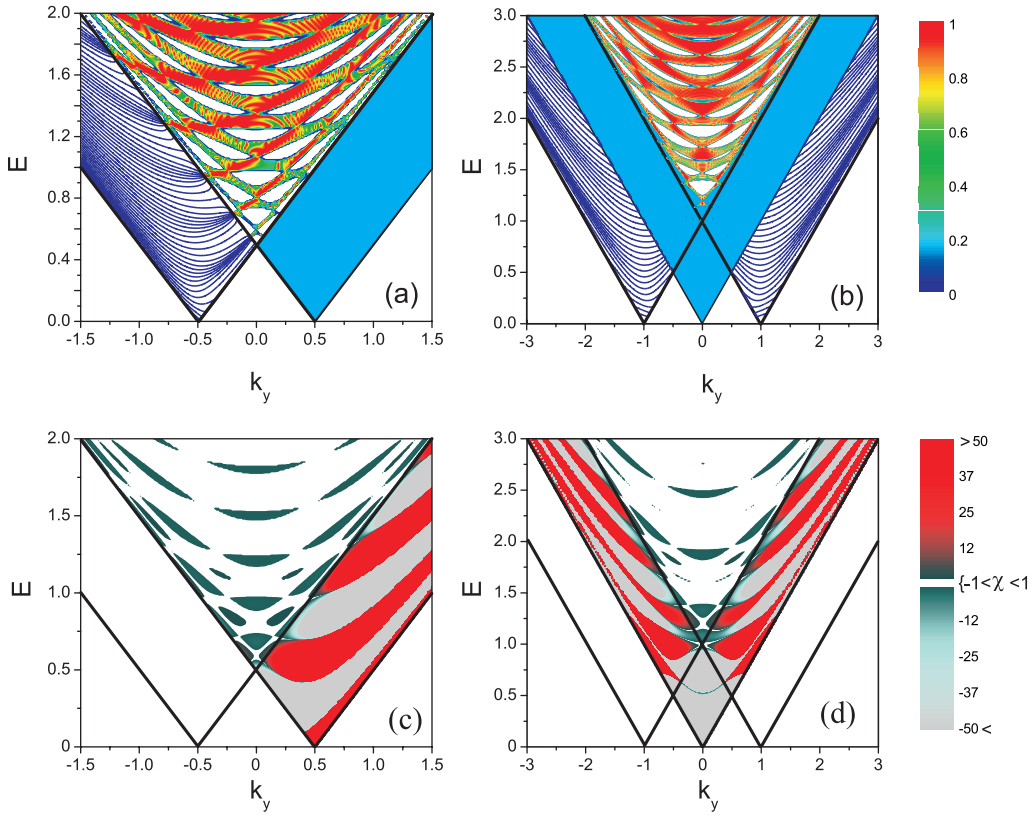

Figure 5. Contour plot of the transmission (a) and Bloch phase (c) through $N = 10$ magnetic δ-function barriers with $a = 10$, $b = 10$ and $P = 1$. (b) and (d) The same as in (a) and (c) for $a = 5$, $b = 5$, $c = 5$, $d = 5$ and $P = 1$, single unit.

the number of barriers increases for both types of units. But the gaps occur when the wave is mostly reflected. The position of these gaps, which are especially pronounced as N increases, can also be found from the structure of the Bloch phase ζ, as shown in figures 5(c) and (d). In figure 5, the bound states are shown by the blue solid curves that are situated in the area $-k_y - P/2 < E < -k_y + P/2$ in case (a) and in $-k_y - P/2 < E < -k_y$ for case (b) plus an area located symmetric with respect to k_y. Notice in figure 5(a) that several bound states merge into a resonant states at $E = -k_y + P/2$. This is different from figure 4(a) where each bound state becomes a resonant state at $E = -k_y$.

3.3. Spectrum of an SL

Let us take $N \to \infty$. We can find the energy-momentum relation from the previous standard calculation [32, 33] by using

$$\cos(k_x L) = \tfrac{1}{2}\,\mathrm{Tr}\,\mathbf{M} = \chi\,, \tag{48}$$

where M is the characteristic matrix of one period. This results in

$$\cos(k_1 a)\cos(k_2 b) - \left(\frac{k_2^2 + k_1^2 + P^2}{2k_2 k_1}\right)\sin(k_1 a)\sin(k_2 b) = \cos k(b+a). \tag{49}$$

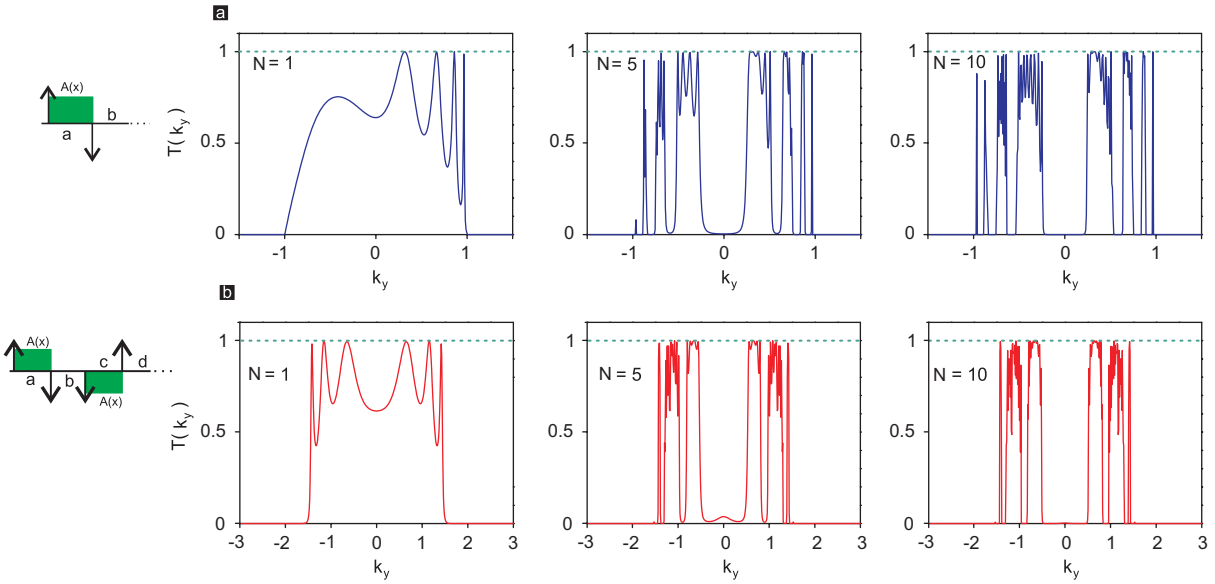

Figure 6. (a) and (b) Transmission versus energy through $N = 1, 5, 10$ magnetic units of δ-function barriers shown on the left. The upper unit has $a = 10$, $b = 10$, $P = 1$, $E = 1.5$ and the bottom one $a = b = c = d = 5$, and $P = 1$ and $E = 2.5$.

With reference to the regions I and II shown in figure 2(a), we write $k_1 = [E^2 - k_y^2]^{1/2}$ and $k_2 = [E^2 - (k_y + P)^2]^{1/2}$ and show the solution for $E^2 > (k_y + P)^2$ in figure 9. Equation (49) differs from the corresponding result of [27], equation (7), for the case of Schrödinger electrons, in the term P^2 in the prefactor of the second term on the right-hand side and the linear E versus k spectrum instead of the quadratic one in [27]. If P is large the differences become more pronounced. Our numerical results for the energy spectrum are shown in figures 7–11. The results for standard and Dirac electrons show not only similarities but also important differences. The first band shows a qualitative difference near $k_y \approx 0$, see figure 9. As figures 7, 9(a) and (b) show, the band behavior in the $k = k_x$ direction for fixed k_y is constant and almost symmetric about $k_y = 0$; the motion becomes nearly 1D for relatively large k_y. From the contour plots of figures 9(b) and (d), as well as from figure 7(c), we infer a collimation along the k_y-direction, i.e. $v_y \propto \partial E/\partial k_y \approx v_F$ and $v_x \approx 0$, which is similar to that found for an SL of electric potential barriers [16] for some specific values of the barrier heights. Also, there are no gaps for $k_y \approx 0$ in figure 10(a) but there are for the case of Dirac electrons as seen in figure 10(b). This difference can be traced back to the presence of P^2 in the dispersion relation equation (49) when compared to the same equation for the standard electron. The even-number energy bands in figure 11(b) are wider than those in figure 11(a) and, as a function of the period, the energy decreases faster for Dirac electrons. This behavior of the bands for Dirac electrons is very similar to that for the frequency ω versus k_y or L in media with a periodically varying refractive index [29]. This is clearly a consequence of the linear $E - k$ relation. Notice the differences between the lowest bands shown in panels (a) and (b) in figure 12 and in particular the difference between the corresponding drift velocities as functions of k_y.

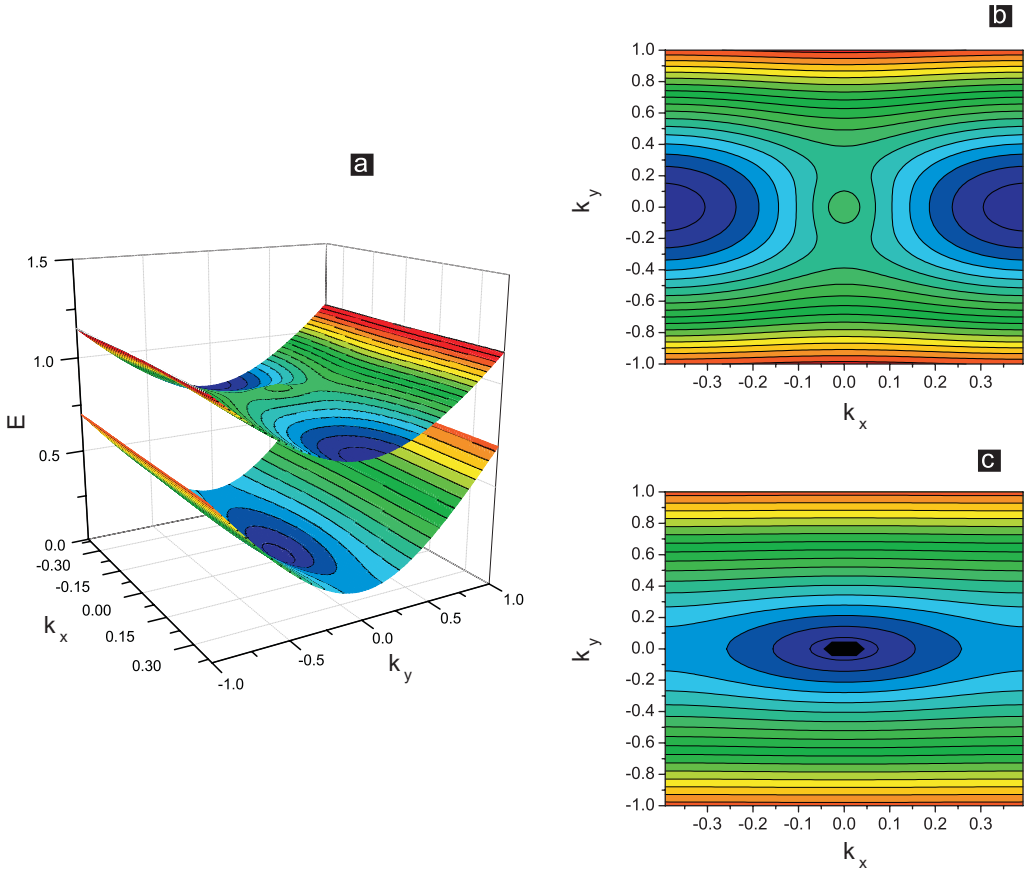

Figure 7. (a) The first two energy bands and contour plot of second (b) and first (c) band for a magnetic SL of δ-function barriers with $a = 4$, $b = 4$, and $P = 1$.

4. A series of δ-function vector potentials

In the limit that the distance between the opposite-directed magnetic barriers decreases to zero the vector potential approaches a δ-function [24]. We consider a series of magnetic δ-function vector potentials $A(x) = \sum_{n=-\infty}^{\infty} A_0\delta(x - nL)$ as shown in figure 11(a). First we consider a single such potential that is zero everywhere except at $x = 0$. We start with equations (6) and (7) which now become

$$-\mathrm{i}\left[\frac{\mathrm{d}}{\mathrm{d}x} + k_y + \ell_\mathrm{B} A_0\delta(x)\right]\phi_\mathrm{b} = E\phi_\mathrm{a}, \tag{50}$$

$$-\mathrm{i}\left[\frac{\mathrm{d}}{\mathrm{d}x} - k_y - \ell_\mathrm{B} A_0\delta(x)\right]\phi_\mathrm{a} = E\phi_\mathrm{b}. \tag{51}$$

The solutions are readily obtained in the form

$$\phi_\mathrm{a} = \begin{cases} A\cos(\varepsilon x\cos\theta) + B\sin(\varepsilon x\cos\theta), & x < 0, \\ C\cos(\varepsilon x\cos\theta) + D\sin(\varepsilon x\cos\theta), & x > 0, \end{cases} \tag{52}$$

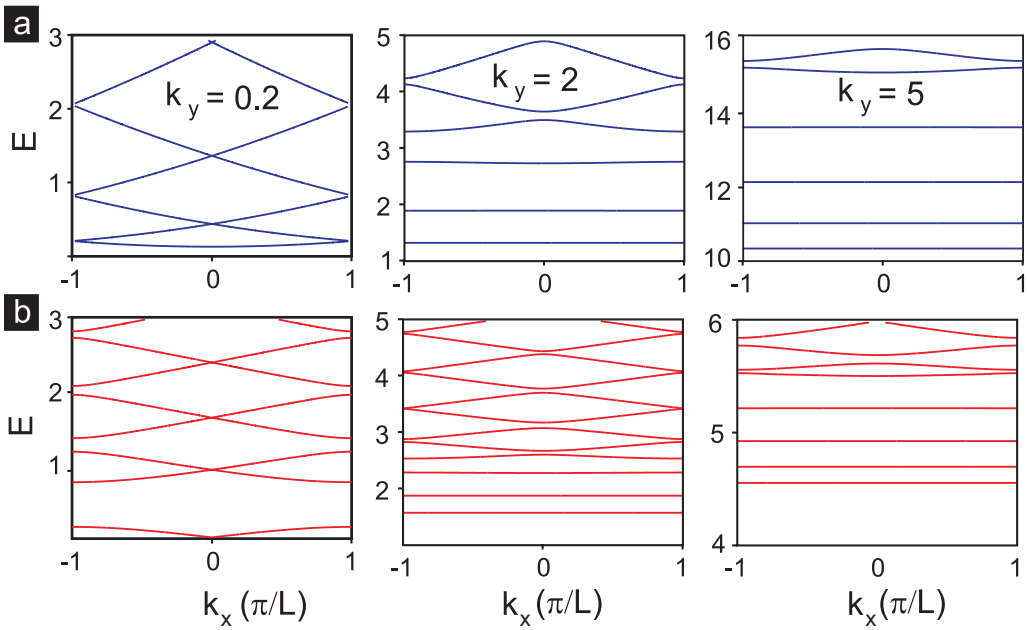

Figure 8. Dispersion relation (E versus k) for a standard electron in (a) and a Dirac electron in (b). The fixed values of k_y are shown in the panels, $L = 8$ and $P = 1$ (the energy for the standard electron is measured in units of $\hbar\omega_c$ with $\omega_c = \sqrt{eB_0/mc}$ and all distances in units of $l_B = \sqrt{c\hbar/eB_0}$).

$$\phi_b = \begin{cases} -i\{B\cos(\theta + \varepsilon x\cos\theta) - A\sin(\theta + \varepsilon x\cos\theta)\}, & x < 0, \\ -i\{D\cos(\theta + \varepsilon x\cos\theta) - C\sin(\theta + \varepsilon x\cos\theta)\}, & x > 0. \end{cases} \tag{53}$$

Integrating equations (50) and (51) around 0 gives

$$-i\int_{0^-}^{0+}\left[\frac{d}{dx} + (k_y + \ell_B A_0\delta(x))\right]\phi_b\,dx = E\int_{0^-}^{0+}\phi_a\,dx, \tag{54}$$

$$-i\int_{0^-}^{0+}\left[\frac{d}{dx} - (k_y + \ell_B A_0\delta(x))\right]\phi_a\,dx = E\int_{0^-}^{0+}\phi_b\,dx \tag{55}$$

and

$$\phi_b(0^-) = \eta\phi_b(0^+), \qquad \phi_a(0^+) = \eta\phi_a(0^-). \tag{56}$$

We now consider the entire series of δ-function vector potentials shown in figure 13(a) and use equations (55) and the periodic boundary condition $\Psi_I(0) = e^{ik_xL}\Psi_{II}(L)$. The resulting dispersion relation for the SL is

$$\cos(kL) = 2\eta(1+\eta^2)^{-1}\cos(k_xL), \tag{57}$$

where $\eta = 1 + \ell_B A_0$. From equation (57) we find the energy spectrum as

$$E_n(k_x, k_y) = \pm\sqrt{2n\pi + k_y^2 + \left(\frac{1}{L}\cos^{-1}\left(\frac{2\eta}{1+\eta^2}\cos(k_xL)\right)\right)^2}. \tag{58}$$

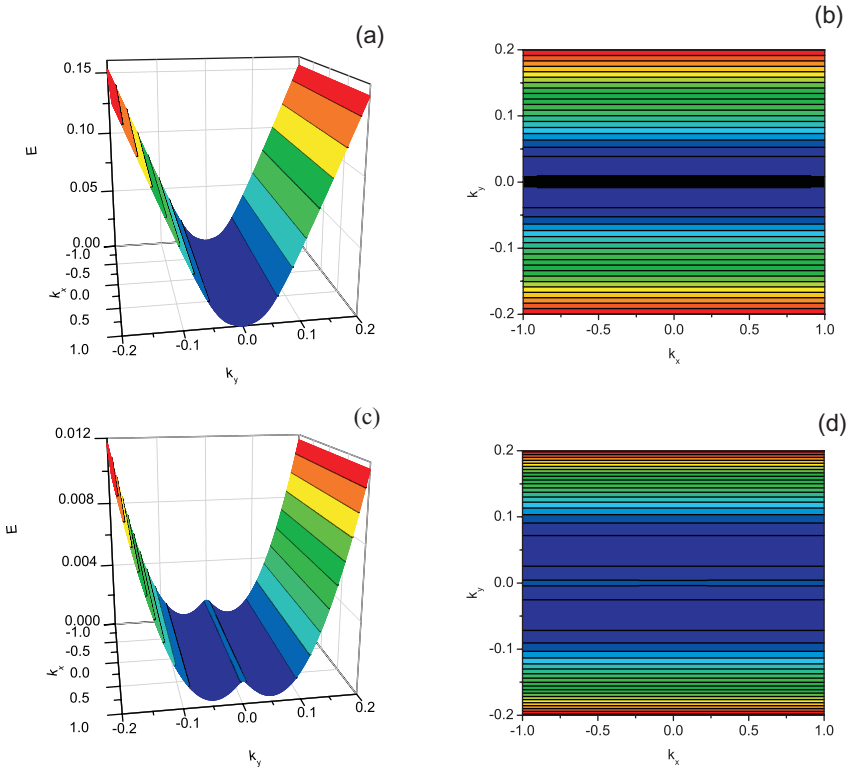

Figure 9. First energy band for (a) standard and (c) Dirac electron in SL of magnetic δ-function barriers with $a = 100$, $b = 100$, and $P = 0.1$. (b) and (d) Corresponding contour plots of (a) and (c) (the energy for the standard electron is measured in units of $\hbar\omega_c$ with $\omega_c = \sqrt{eB_0/mc}$ and all distances in units of $l_B = \sqrt{c\hbar/eB_0}$).

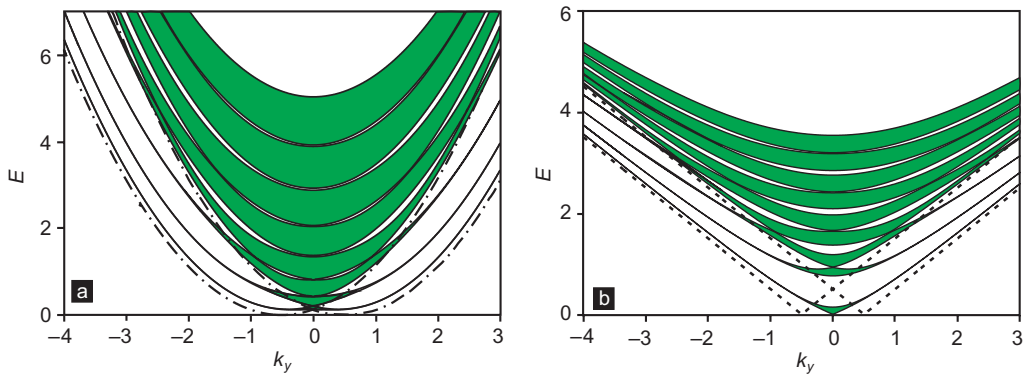

Figure 10. Dispersion relation for (a) a standard electron and (b) a Dirac electron. The period is $L = a + b = 8$ and the shaded (in green) regions are the lowest six allowed bands. The solid curves in both panels, the dash-dotted curves in (a) and the dashed ones in (b) show bound states for a free electron (the energy for the standard electron is measured in units of $\hbar\omega_c$ with $\omega_c = \sqrt{eB_0/mc}$ and all distances in units of $l_B = \sqrt{c\hbar/eB_0}$).

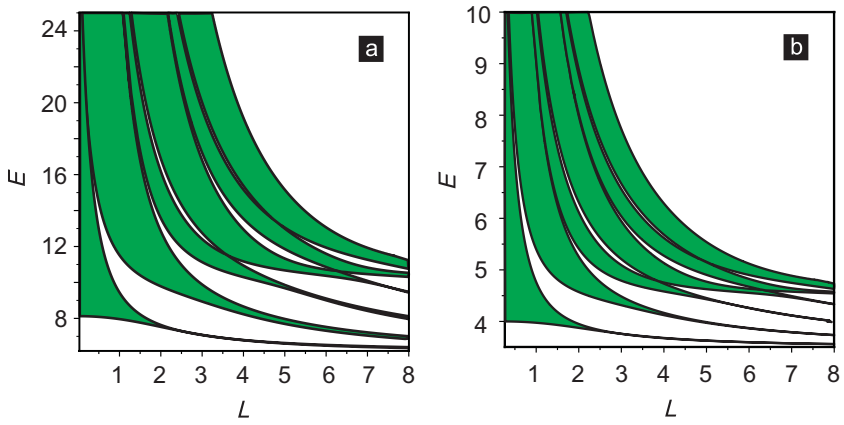

Figure 11. Energy versus period $L = a + b$ for (a) a standard electron and (b) a Dirac electron with fixed $k_y = 4$ (the energy for the standard electron is measured in units of $\hbar\omega_c$ with $\omega_c = \sqrt{eB_0/mc}$ and all distances in units of $l_B = \sqrt{c\hbar/eB_0}$).

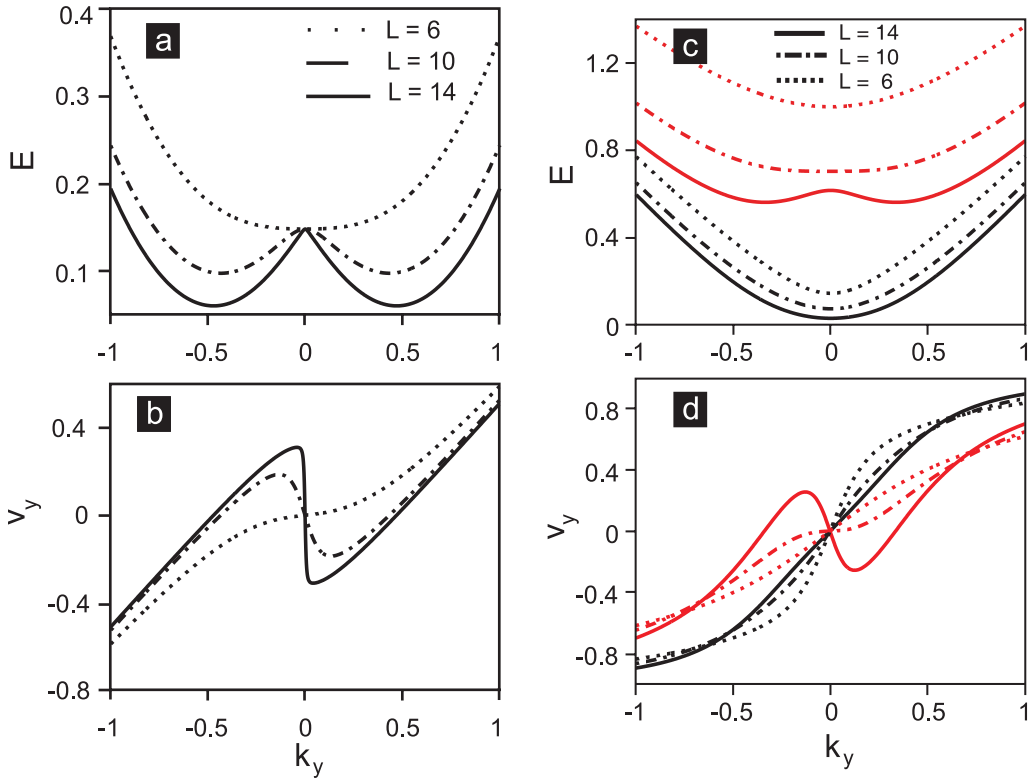

Figure 12. (a) and (b) Lowest-energy band for a standard electrons and drift velocity versus k_y for three different values of L. (c) and (d) First (black curves) and second (red curves) band for Dirac electrons and the drift velocity versus k_y for three different values of L (the energy for the standard electron is measured in units of $\hbar\omega_c$ with $\omega_c = \sqrt{eB_0/mc}$ and all distances in units of $l_B = \sqrt{c\hbar/eB_0}$).

We can define

$$(1/L)\cos^{-1}\left[2\eta(1+\eta^2)^{-1}\cos(k_x L)\right] = s \tag{59}$$

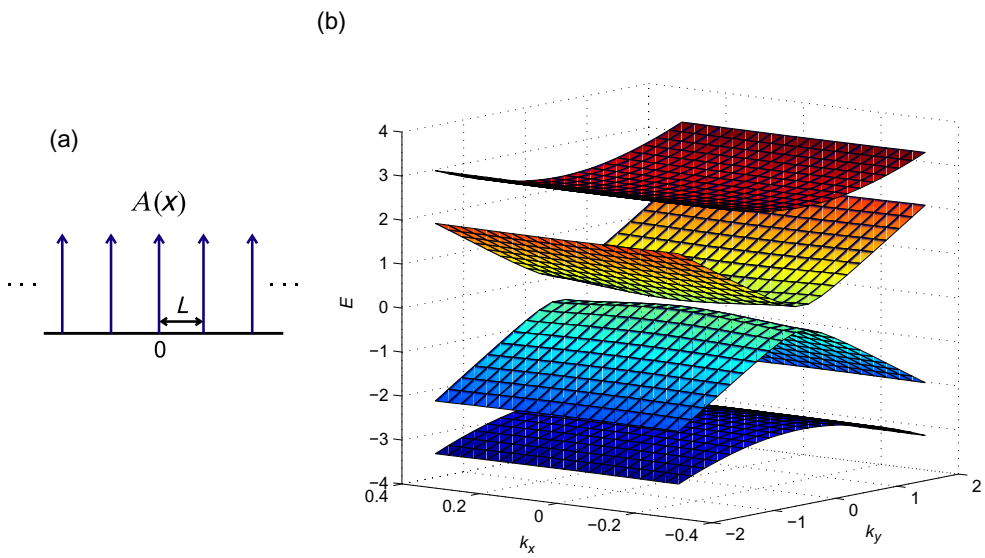

Figure 13. (a) A series of δ-function vector potentials. (b) Dispersion relation for the system shown in (a).

and obtain

$$E = \pm[2n\pi + k_y^2 + s^2]^{1/2}. \tag{60}$$

The energy bands around the Dirac point are plotted in figure 12(b). Notice that: (i) there is an opening of a gap at the Dirac point, (ii) the motion is strongly 1D, i.e. along the k_y-direction, and (iii) higher subbands have a smaller dispersion.

5. Concluding remarks

We developed a *magnetic* KP model for Dirac electrons in graphene. The model is essentially a series of very high and very narrow *magnetic* δ-function barriers alternating in sign. The treatment of the transmission through such a series of barriers followed closely the one developed in optics for media in which the refractive index varies in space [28, 29]. We contrasted a few of the results with those for standard electrons described by the Schrödinger equation [27].

In several cases the energy spectrum or the dispersion relation was obtained analytically, cf equations (25), (39), (47), (48) and (57), largely due to the simplicity of the model and the adapted method from optics. For only two *magnetic* δ-function barriers, opposite in sign, we saw several bound states, whose number increases with $|k_y|$, and a reduction of the wavevector range for which tunneling is possible, cf figure 4(a). This is in line with that reported earlier for single [7] and multiple [9] barriers. The reduction becomes stronger as we increase the number of barriers, cf figure 4(b). We also made contact with Snell's law in optics, cf equation (36): the term P/E represents the deviation from this law.

An important feature of the SL results is a collimation of an incident electron beam normal to the superlattice direction at least for large wavevectors. As easily seen from figures 7 and 8, for $|k_y| \geqslant 2$ we have $v_x \propto \partial E/\partial k_x \approx 0$ for the first three minibands in the middle panels

and nearly five minibands in the right panels. This occurs for both standard electrons and Dirac electrons, but notice the important difference for $|k_y| \approx 0$ shown clearly in figure 9. This collimation is similar to that reported in [16] for SLs involving only electric barriers but with somewhat unrealistic large barrier heights.

It is also worth emphasizing the differences and similarities in the first two minibands and the corresponding drift velocities as functions of k_y for different periods L and constant k_x as shown in figure 12. Notice, in particular, the resemblance between the drift velocities in the lowest miniband for standard electrons and the second miniband for Dirac electrons.

Given that ferromagnetic strips were successfully deposited on the top of a 2DEG in a semiconductor heterostructure [23], we hope they will be deposited on graphene too and that the results of this paper will be tested in the near future.

Acknowledgments

We thank Professor A Matulis for helpful discussions. This work was supported by the Flemish Science Foundation (FWO-Vl), the Belgian Science Policy (IAP), the Brazilian National Research Council CNPq and the Canadian NSERC Grant No. OGP0121756.

References

[1] Novoselov K S, Geim A K, Morozov S V, Jiang D, Katsnelson M I, Grigorieva I V, Dubonos S V and Firsov A A 2005 *Nature* **438** 197
[2] Zheng Y, Tan Y W, Stormer H L and Kim P 2005 *Nature* **438** 201
[3] Katsnelson M I, Novoselov K S and Geim A K 2006 *Nat. Phys.* **2** 620
Milton Pereira Jr J, Vasilopoulos P and Peeters F M 2007 *Appl. Phys. Lett.* **90** 132122
[4] Peeters F M and Matulis A 1993 *Phys. Rev.* B **48** 15166
[5] Reijniers J, Peeters F M and Matulis A 2001 *Phys. Rev.* B **64** 245314
[6] Reijniers J, Peeters F M and Matulis A 1999 *Phys. Rev.* B **59** 2817
[7] De Martino A, Dell'Anna L and Egger R 2007 *Phys. Rev. Lett.* **98** 066802
[8] Ramezani Masir M, Vasilopoulos P, Matulis A and Peeters F M 2008 *Phys. Rev.* B **77** 235443
[9] Ramezani Masir M, Vasilopoulos P and Peeters F M 2008 *Appl. Phys. Lett.* **93** 242103
[10] Park S and Sim H S 2008 *Phys. Rev.* B **77** 075433
[11] Oroszlany L, Rakyta P, Kormanyos A, Lambert C J and Cserti J 2008 *Phys. Rev.* B **77** 081403
[12] Ghosh T K, De Martino A, Häusler W, Dell'Anna L and Egger R 2008 *Phys. Rev.* B **77** 081404
[13] Zhai F and Chang K 2008 *Phys. Rev.* B **77** 113409
[14] Tahir M and Sabeeh K 2008 *Phys. Rev.* B **77** 195421
[15] Xu H, Heinzel T, Evaldsson M and Zozoulenko I V 2008 *Phys. Rev.* B **77** 245401
[16] Park C-H, Giustino F, Cohen M L and Louie S G 2009 *Nano Lett.* **9** 1731
[17] van Houten H, van Wees B J, Mooij J E, Beenakker C W J, Williamson J G and Foxon C T 1988 *Europhys. Lett.* **5** 721
[18] Spector J, Stormer H L, Baldwin K W, Pfeiffer L N and West K W 1990 *Appl. Phys. Lett.* **56** 1290
[19] Sivan U, Heiblum M, Umbach C P and Shtrikman H 1990 *Phys. Rev.* B **41** R7937
[20] Molenkamp L W, Staring A A M, Beenakker C W J, Eppenga R, Timmering C E, Williamson J G, Harmans C J P M and Foxon C T 1990 *Phys. Rev.* B **41** R1274
[21] Yacoby A, Heiblum M, Umansky V, Shtrikman H and Mahalu D 1994 *Phys. Rev. Lett.* **73** 3149
[22] Matulis A, Peeters F M and Vasilopoulos P 1994 *Phys. Rev. Lett.* **72** 1518
[23] Nogaret A, Lawton D N, Maude D K, Portal J C and Henini M 2003 *Phys. Rev.* B **67** 165317
[24] Pereira V M and Castro Neto A H 2009 *Phys. Rev. Lett.* **103** 046801

[25] Ghosh S and Sharma M 2009 *J. Phys.: Condens. Matter* **21** 292204
[26] Dell'Anna L and Martino A D 2009 *Phys. Rev.* B **79** 045420
[27] Ibrahim I S and Peeters F M 1995 *Phys. Rev.* B **52** 17321
Ibrahim I S and Peeters F M 1995 *Am. J. Phys.* **63** 171
[28] Born M and Wolf E 1980 *Principles of Optics* (Oxford: Pergamon)
[29] Yariv A 1976 *Optical Waves in Crystals* (New York: Wiley)
[30] Ponomarenko L A, Schedin F, Katsnelson M I, Yang R, Hill E W, Novoselov K S and Geim A K 2008 *Science* **320** 356
[31] Cheianov V V, Faĺko V and Altshuler B L 2007 *Science* **315** 1252
[32] McKellar B H J and Stephenson G J Jr 1987 *Phys. Rev.* C **35** 2262
[33] Griffiths D J and Steinke C A 2001 *Am. J. Phys.* **69** 137